An in silico cardiomyocyte reveals the impact of changes in CAMKII signalling on cardiomyocyte kinetics in hypertrophic cardiomyopathy

Ismail Adeniran[a]*, Hans Degens[b,c]
[a] Centre for Advanced Computational Science, Manchester Metropolitan University, Manchester M15 6BH, United Kingdom
[b] Musculoskeletal and Sports Medicine, Manchester Metropolitan University, Manchester M15 6BH, United Kingdom
[c] Lithuanian Sports University, Kaunas, Lithuania
Correspondence address: i.adeniran@mmu.ac.uk

Abstract
Hypertrophic cardiomyopathy (HCM) is characterised by asymmetric left ventricular hypertrophy, ventricular arrhythmias and cardiomyocyte dysfunction that may cause sudden death. HCM is associated with mutations in sarcomeric proteins and is usually transmitted as an autosomal-dominant trait. The aim of this *in silico* study was to assess the mechanisms by which HCM alters electrophysiological activity, contractility, energy metabolism regulation and crossbridge cycling at the single cell level. To investigate this, we developed a human ventricular cardiomyocyte model that incorporates electrophysiology, metabolism and force generation. The model was validated by its ability to reproduce the experimentally observed kinetic properties of human HCM induced by a) remodelling of several ion channels and Ca^{2+} handling proteins arising from altered Ca^{2+}/calmodulin kinase II signalling pathways; and b) increased Ca^{2+} sensitivity of the myofilament proteins. Our simulation showed a decreased phosphocreatine to ATP ratio (-9%) suggesting a negative mismatch between energy expenditure and supply. Using a spatial, myofilament half sarcomere model, we also compared the fraction of detached, weakly bound and strongly bound crossbridges in the control and HCM conditions. Our simulations showed that HCM has more crossbridges in force producing states than in the control condition. In conclusion, our model reveals that impaired crossbridge kinetics is accompanied by a negative mismatch between the ATP supply : demand ratio. This suggests that improving this ratio may reduce the incidence of sudden death in HCM.

Keywords: hypertrophic cardiomyopathy, in silico, cardiomyocyte, sarcomere, energetics, multifilament, crossbridge cycling

1 Introduction

Hypertrophic cardiomyopathy (HCM) is the most common inherited cardiac disorder, affecting 1 in 500 individuals, and is clinically characterised by left ventricular (LV) hypertrophy, a decrease in the LV chamber size, heart failure, arrhythmias and sudden cardiac death at any age (Pasipoularides, 2018; Semsarian, 2018; Spudich, 2014). While the Ejection Fraction (EF) is preserved, the rate of relaxation is diminished (Haland et al., 2017; Marian and Braunwald, 2017; Spudich, 2014). It usually results from mutations of sarcomeric proteins; the sarcomere being the fundamental contractile unit of the cardiomyocyte (Pasipoularides, 2018; Spudich, 2014). Histopathology features include disorganized myocyte architecture, including disarray of myocyte fibres, intertwined hypertrophied myocytes, and focal or widespread interstitial fibrosis (Rowin and Fifer, 2021; Tejado and Jou, n.d.).

Over the past two decades, it has been suggested that an energy deficit plays an essential role in the aetiology of HCM (Ormerod et al., 2016; Pasipoularides, 2018; Ranjbarvaziri et al., 2021; Wijnker et al., 2019). Most mutations in HCM lead to an increase in both the total force production and adenosine triphosphate (ATP) utilisation at the cellular level, consequently leading to a greater ATP demand by the cardiomyocytes (Ashrafian et al., 2003; Ranjbarvaziri et al., 2021). Yet, notwithstanding this increased demand for ATP, both murine models (Lucas et al., 2003; Tardiff et al., 1999) and patients (Unno et al., 2009) with HCM have found an impaired, rather than enhanced, mitochondrial function and morphology. Despite significant advances in elucidating sarcomeric structure–function relationships and evidence linking impaired energy metabolism with the aetiology of HCM, there is still much to be discovered about the mechanisms that link altered cardiac energetics to HCM phenotypes due to insufficient cell and animal models and more importantly, human HCM patient studies (Li et al., 2018; Ranjbarvaziri et al., 2021).

Studies indicate that the pathogenesis of HCM involves a broad range of mechanisms; the primary mechanism of which is sarcomeric protein mutation. Molecular changes that occur in response to the changes in the sarcomere protein structure and function form a secondary mechanism with histological and pathological phenotypes as a consequence of the molecular perturbations being tertiary mechanisms (Marian and Braunwald, 2017; Pasipoularides, 2018; Ranjbarvaziri et al., 2021; Rowin and Fifer, 2021). One such tertiary mechanism may be the complex remodelling process involving alterations of Ca^{2+}/calmodulin-dependent protein kinase II (CAMKII)-dependent signalling that is not a direct consequence of sarcomeric mutations (Coppini et al., 2018, 2013). In this study, we investigated how functional changes in CAMKII-dependent signalling alter electrophysiological activity, contractility and energy metabolism regulation at the level of the single cardiomyocyte in human HCM.

2 Materials and Methods

2.1 Electromechanical, Mitochondrial Energetics Single Cell Model

We employed the O'Hara-Rudy (ORd) human ventricular single cell model (O'Hara et al., 2011) for electrophysiology (EP). This model is based on undiseased human ventricular data and accurately reproduces the electrical and membrane channel characteristics of human ventricular cells, as well as the transmural heterogeneity of ventricular action potentials (AP) across the ventricular wall. Furthermore, the ORd model also replicates the Ca^{2+} vs. voltage-dependent inactivation of the L-type Ca^{2+} current and modulation of the rate of Ca^{2+} cycling by CaMK.

To simulate cellular contractile properties, we utilised the myofilament model developed by Tran et al. (Tran et al., 2010). This model was selected because it is an extension of the Rice et al. cross-bridge cycling model (Rice et al., 2008), which is a widely recognised and established model of cardiac muscle contraction. Not only can the myofilament model replicate a variety of experimental data, such as steady-state force-sarcomere length (F-SL), force-Ca^{2+}, and sarcomere length- Ca^{2+} relationships but it can also reproduce many of the effects on force development due to MgATP, MgADP, Pi and H^+ (Rice et al., 2008; Tran et al., 2010).

The EP model's intracellular calcium concentration $[Ca^{2+}]_i$ served as the link between the EP model and the myofilament model. Specifically, the dynamic $[Ca^{2+}]_i$ generated by the EP

model during the AP was used as input to the myofilament model, which then calculated the quantity of Ca^{2+} bound to troponin. The myoplasmic $[Ca^{2+}]_i$ concentration in the human ventricular myocyte electromechanical cell model is formulated accordingly:

$$\frac{d[Ca^{2+}]_i}{dt} = \beta_{Cai} \cdot \left(-\left(I_{pCa} + I_{Cab} - 2 \cdot I_{NaCa,i}\right) \cdot \frac{A_{cap}}{2 \cdot F \cdot v_{myo}} - J_{up} \cdot \frac{v_{nsr}}{v_{myo}} + J_{diff,Ca} \cdot \frac{v_{ss}}{v_{myo}} - \frac{J_{Trop}}{1000} \right) \quad (1)$$

where β_{Cai} is the buffer factor for $[Ca^{2+}]_i$, I_{pCa} (μA/μF) is the sarcolemmal Ca^{2+} pump current, I_{Cab} (μA/μF) is the Ca^{2+} background current, $I_{NaCa,i}$ (μA/μF) is the myoplasmic component of Na^{+}/Ca^{2+} exchange current, A_{cap} (cm^2) is capacitive area, F (Coulomb/mol) is the Faraday constant, v_{myo} (μL) is the volume of the myoplasmic compartment, v_{nsr} (μL) is the volume of the sarcoplasmic reticulum compartment, v_{ss} (μL) is the volume of the subspace compartment, J_{up} (mM/ms) is the total Ca^{2+} uptake flux via the SERCA pump from myoplasm to the sarcoplasmic reticulum, $J_{diff,Ca}$ (mM/ms) is the diffusion flux of Ca^{2+} from the subspace to the myoplasm and J_{Trop} (μM/ms) is the flux of Ca^{2+} binding to troponin. β_{Cai} is formulated as:

$$\beta_{Cai} = \frac{1}{1 + \frac{[CMDN] \cdot K_{m,CMDN}}{\left(K_{m,CMDN} + [Ca^{2+}]_i\right)^2}} \quad (2)$$

where [CMDN] is the calmodulin Ca^{2+} buffer in the myoplasm and $K_{m,CMDN}$ is the half-saturation concentration of calmodulin.

For cardiac mitochondrial bioenergetics, we then coupled this electromechanical single cell model to the thermokinetic, mitochondrial model of Cortassa et al. (Cortassa et al., 2003). This model describes the tricarboxylic acid (TCA) cycle, oxidative phosphorylation and mitochondrial Ca^{2+} handling. It can reproduce, qualitatively and semi-quantitatively, experimental data concerning mitochondrial bioenergetics, Ca^{2+} dynamics and respiratory control. The sarcolemmal Ca^{2+} pump current (I_{pCa}) and the SERCA pump uptake flux (J_{up}) of the electromechanical single cell model was modified to take into account mitochondrial energetics as follows:

$$I_{pCa} = G_{pCa} \cdot \frac{[Ca^{2+}]_i}{0.0005 + [Ca^{2+}]_i} \cdot \frac{1}{1 + \left(\frac{K_{m1_pCa}^{ATP}}{[ATP]_i}\right) \cdot \left(1 + \frac{[ADP]_i}{K_{i_pCa}^{ADP}}\right)} + \frac{1}{1 + \left(\frac{K_{m2_pCa}^{ATP}}{[ATP]_i}\right)} \quad (3)$$

where G_{pCa} is the maximum conductance of I_{pCa}, $K_{m1_pCa}^{ATP}$ is the first ATP (adenosine triphosphate) half saturation constant for I_{pCa}, $K_{m2_pCa}^{ATP}$ is the second ATP half saturation constant for I_{pCa}, $K_{i_pCa}^{ADP}$ is the ADP inhibition constant for I_{pCa}, $[ATP]_I$ is the excitation-

contraction (EC) coupling linked ATP concentration and $[ADP]_I$ is the excitation-contraction (EC) coupling-linked ADP (adenosine diphosphate) concentration.

$$J_{up} = \left(\left(1 - \emptyset_{up,CaMK}\right) \cdot J_{up,NP} + \emptyset_{up,CaMK} \cdot J_{up,CaMK} - J_{leak}\right) \cdot \left(\frac{\left(K_{SR}^{mATP} + [ADP]_i \cdot K_{SR_Ki_SR}^{mATP}\right)}{[ATP]_i} + \left(1 + \frac{[ADP]_i}{Ki'_{SR}}\right)\right) \quad (4)$$

where $\emptyset_{up,\ CaMK}$ is the fraction of channels phosphorylated by CaMK, $J_{up,NP}$ is the non-phosphorylated Ca^{2+} uptake by CaMK via SERCA pump, $J_{up,CaMK}$ is the CaMK phosphorylated Ca^{2+} uptake via SERCA pump and J_{leak} is the leakage flux.

2.2 HCM Electromechanical Single Cell Model

To develop the human electromechanical single cell model of a HCM cardiomyocyte, we first modified the EP and myofilament models to reflect Coppini et al's (Coppini et al., 2018, 2013) experimental data on the electromechanical profile of cardiomyocytes from 26 HCM patients. We made the following changes to the electromechanical single cell model (Table 1).

Parameter	HCM
Volume	+100%
Capacitance	+59%
G_{NaL}	+107%
G_{Kr}	-34%
G_{Ks}	-27%
G_{to}	-85%
G_{K1}	-15%
G_{CaL}	+19%
G_{NaCa}	+34%
SERCA	-43%
CAMKa	+350%
PLB	-40%
***Hill Coefficient**	-50%

Table 1: HCM functional changes (Coppini et al., 2018, 2013) made to the electromechanical single cell model. *Change made to the myofilament model of the coupled single model. G_{NaL} is the maximum conductance of the late sodium current, G_{Kr} is the maximum conductance of the rapid delayed rectifier K^+ current, G_{Ks} is the maximum conductance of the slow delayed rectifier K^+ current, G_{Kr} is the maximum conductance of the rapid delayed rectifier K^+ current, G_{to} is the maximum conductance of the transient outward K^+ current, G_{K1} is the maximum conductance of the inward rectifier K^+ current, G_{CaL} is the maximum conductance of the Ca^{2+} current through the L-type Ca^{2+} channel, G_{NaCa} is the maximum conductance of the Na^+/K^+ exchange current, SERCA is the sarco/endoplasmic reticulum Ca^{2+}-ATPase pump, CaMKa is the fraction of active Ca^{2+}/calmodulin-dependent protein kinase II binding sites, PLB is phospholamban and the Hill coefficient is a measure of the calcium sensitivity of the cardiomyocyte.

2.3 Spatially Explicit, Half-sarcomere Multifilament Model

To further investigate how HCM drives pathological behaviour, we also employed a spatially explicit, multifilament computational model of the half sarcomere (Powers et al., 2018; Williams et al., 2013, 2012, 2010). The model is comprised of eight actin filaments and four myosin filaments arranged in a three-dimensional double-hexagonal lattice (Figs 1A and 1B). It simulates an infinite lattice using periodic (toroidal) boundary conditions (Fig. 1B). It models each cross-bridge as a two-spring system consisting of a torsional and linear component. Linear springs are connected in series between each node of cross-bridge crowns for the myosin and actin filaments (Fig. 1C). Each myosin filament contains 60 crowns of three myosin motors (180 cross-bridges per myosin filament). Importantly, the new model possesses two noteworthy characteristics that distinguish it from other existing models: first, it integrates torsional springs and lever-arm mechanisms that expose a correlation between step size and lattice spacing. Second, this lever-arm mechanism generates both radial and axial forces of similar magnitude, mirroring experimental findings (Williams et al., 2010).

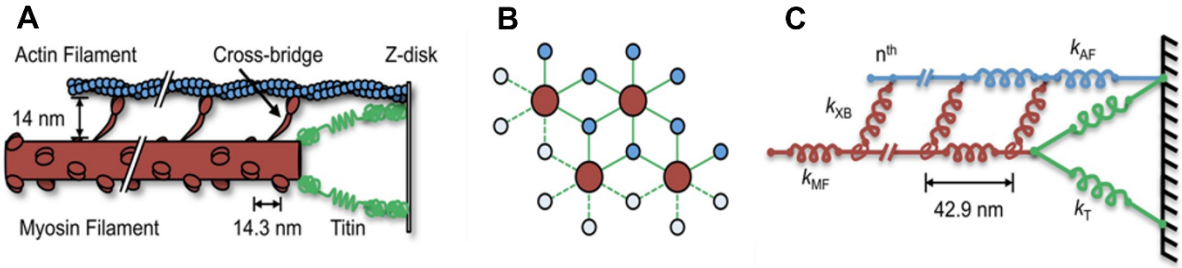

Figure 1: Spatially explicit, half sarcomere model (modified from (Powers et al., 2018)). **(A)** Schematic of the half sarcomere showing myosin filament (red), actin filament (blue), titin (green), z-disk (black) and crossbridges (red). **(B)** Spatial hexagonal arrangement of myosin and actin filaments. **(C)** Mathematically, the half sarcomere is modelled as an array of springs: myosin and crossbridges (red), actin (blue) and titin (green).

As input to the multifilament, half sarcomere model, we digitised $[Ca^{2+}]_i$ transients recorded from control and HCM cardiomyocytes in Coppini et al.'s (Coppini et al., 2018, 2013) study on 26 HCM patients (Fig. 2A). We also digitised and used as input a second set of recorded $[Ca^{2+}]_i$ transients from control and HCM cardiomyocytes with a myosin binding protein C (MYBPC3) mutation (Fig. 2B) from Pioner et al.'s study on 93 HCM patients (Pioner et al., 2023). Mutations to MYBPC3 are the most common cause of HCM (Helms et al., 2020). In each case, the maximum $[Ca^{2+}]_i$ for the control condition was set equivalent to an actin permissiveness of 1 during crossbridge cycling while the minimum $[Ca^{2+}]_i$ for the control condition was set equivalent to an actin permissiveness of 0.2. Values of actin permissiveness were proportionally adjusted between these values during the time course simulation of the pre-recorded profiles for both control and HCM conditions. Each time point of each calcium transient profile was run for 100ms until steady state after which the steady values of the active force and fraction of crossbridges in the strongly bound, weakly bound and detached states were recorded (Fig. 5).

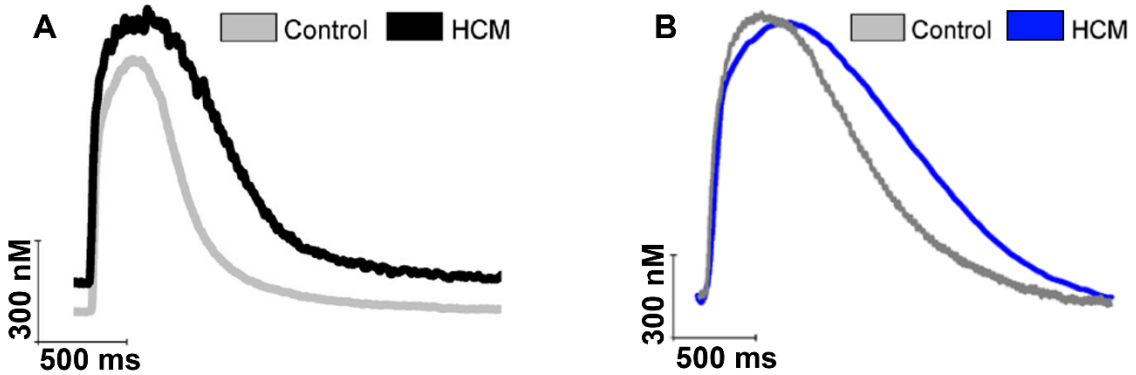

Figure 2: $[Ca^{2+}]_i$ transients recorded from control and HCM cardiomyocytes input into the multifilament half-sarcomere model (modified from (Coppini et al., 2013; Pioner et al., 2023). (**A**) Transients recorded from in current clamp mode in a study on 26 HCM patients (Coppini et al., 2013). **(B)** Transients recorded from study on 96 patients with a MYBPC3 mutation (Pioner et al., 2023).

3. Results and Discussion

3.1 Model Validation: HCM Electromechanical Single Cell

To validate the HCM single cell model, we computed a steady-state force- Ca^{2+} (F-pCa) relationship for a sarcomere length (SL) of 2.2 µm for comparison with the experimental data (Coppini et al., 2013). The results are shown in Figure 3. The model reproduced the differences in total and passive forces between control and HCM, which matched experimental data (inset).

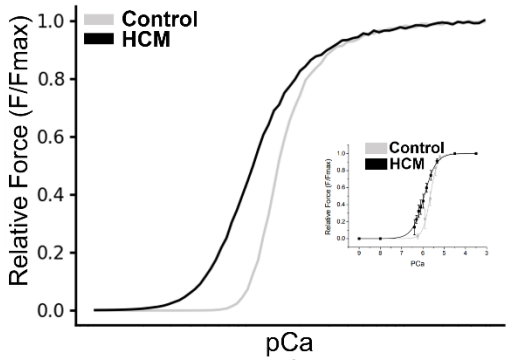

Figure 3: Force-pCa Relationship. Simulated Force-pCa relationship in control and HCM. Relative force is normalised to maximum value that can be attained. Inset: Experimental force-pCa relation of skinned HCM and control preparations obtained from human patients (Coppini et al., 2013).

3.2 Functional Electrophysiological Consequences of HCM

Figure 4 shows the electromechanical consequences of HCM in a free-running cell from the epicardium. HCM increased the action potential duration (APD_{90}) from 231 ms to 342 ms (Fig. A, E, I). This is qualitatively similar to what was experimentally observed in HCM cardiomyocytes (Coppini et al., 2013).

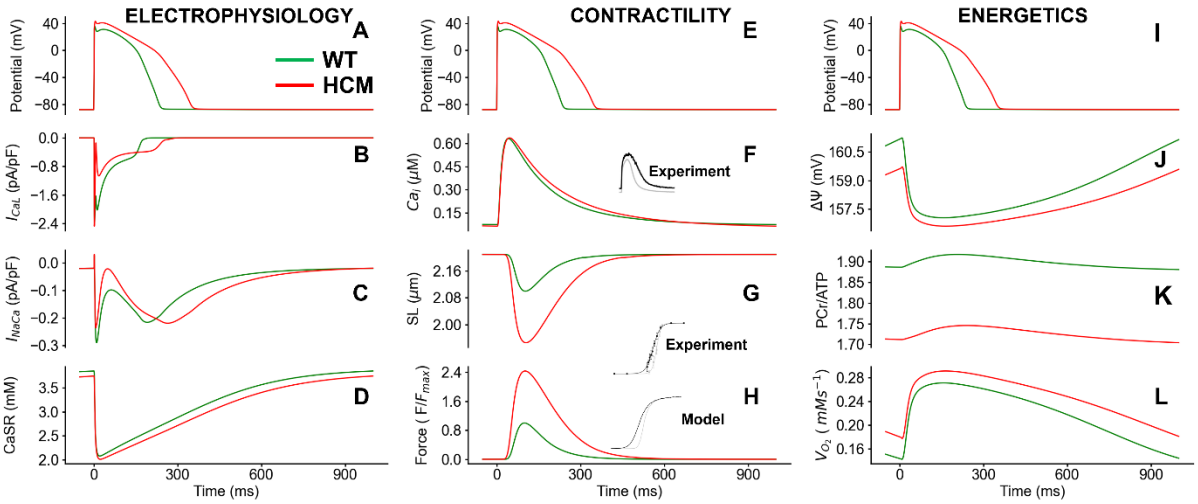

Figure 4 (Colour): Electrophysiological (A-D), contractile (E-H) and bioenergetics (I-L) properties under control (grey) and HCM (black) at 1Hz cycle length. **(A, E, D):** Epicardial action potentials in HCM and control. **(B)** L-type Ca^{2+} channel current (I_{CaL}). **(C)** Sodium/calcium exchange current (I_{NaCa}). **(D)** Ca^{2+} release from the sarcoplasmic reticulum. **(F)** $[Ca^{2+}]_i$ transients. **(G)** Sarcomere length (SL). **(H)** Active force. Values are normalised to Control maximum active force. **(J)** Time rate of change of mitochondrial membrane potential. **(K)** Phosphocreatine to ATP (PCr/ATP ratio. **(L)** Oxygen consumption rate (V_{02}).

The L-type Ca^{2+} current density (I_{CaL}) was increased in HCM at the onset of AP depolarisation but reduced in amplitude during the plateau phase (Figure 4B). The intracellular Ca^{2+} concentration $[Ca^{2+}]_i$ amplitude was similar in HCM and control (Figure 4F) but its kinetics was slower in HCM. The slowed kinetics of $[Ca^{2+}]_i$ (Figure 4F) coupled with the transient increase in I_{CaL}, led to the increased the amplitude of the reverse-mode of the Na^+/Ca^{2+} exchanger (NCX) with its forward mode unchanged (Figure 4C). This resulted in a reduced sarcoplasmic reticulum (SR) content in HCM (Figure 4D), and consequently leading to a smaller SR Ca^{2+} release as demonstrated by the reduced SR content. In association with the decreased conductances of the repolarising K^+ currents (Table 1; G_{Kr}, G_{Ks}, G_{to}, G_{K1}), these served to prolong the action potential in HCM (Figure 4A).

With every heartbeat, the $[Ca^{2+}]_i$ undergoes an order of magnitude change, while the resulting force may change by three or more orders of magnitude. This biological design is believed to be motivated by the need for significant changes in developed force to efficiently pump blood. When incomplete relaxation occurs, a residual force, and hence pressure in the ventricle, inhibits proper filling during diastole, resulting in the ejection of only a small amount of blood during systole. In contrast, cardiac cells produce relatively changes in $[Ca^{2+}]_i$ because ATP energy is required to actively increase and decrease $[Ca^{2+}]_i$ with each heartbeat. Thus, the steep nonlinearity of the F-pCa relationship bridges the gap between the small change in $[Ca^{2+}]_i$ and the large changes in force. A steep nonlinearity enables a much larger relative change in force for a much smaller relative change in $[Ca^{2+}]_i$ per heartbeat (Chung et al., 2016; Sun and Irving, 2010). Figure 3 shows that the force-pCa relationship is left-shifted in HCM patients indicating increased Ca^{2+} sensitivity, which resulted in greater sarcomere length shortening (Fig. 4G) and consequently, greater developed force in HCM (Fig. 4H).

The mitochondrion is a major storage organism of Ca^{2+} and regulates the intracellular Ca^{2+} homeostasis with the SR (Santo-Domingo and Demaurex, 2010). The mitochondrial membrane potential ($\Delta\Psi$) is an essential component in the process of energy storage during oxidative phosphorylation and is intrinsic to the manufacture of ATP (Santo-Domingo and Demaurex, 2010; Zorova et al., 2018). $\Delta\Psi$ was reduced in HCM (Fig. 4J), implying a lowered electron transport chain oxygen radical and hence, energy expenditure beyond supply (Figure 4J). The inefficient energy usage can be observed in the tension cost - impaired energy metabolism, as indicated by a decreased phosphocreatine to ATP ratio (-9%) (Figure 4K) and the increased oxygen consumption rate, i.e., the respiration rate (Figure 4L). The ratio of phosphocreatine/ATP reflects the availability of phosphocreatine and is a measure of the energy state of the myocardium (Del Franco et al., 2022; Henry et al., 2022; S et al., 1997). The impaired cardiac energetics in HCM resulting from our model has been tested and seen in a multiomics profile study of 27 HCM patients and 13 controls (Ranjbarvaziri et al., 2021) lending validity to our results and the developed human, electromechanical, energetic single cell model.

3.3 Functional Consequences of HCM on Crossbridge Cycling

Using the spatial, multifilament, half sarcomere model (Powers et al., 2018; Williams et al., 2013, 2012, 2010), we further investigated the functional consequences of HCM on crossbridge cycling. The half sarcomere model is a three-state model with states for crossbridge attachment, force generation and detachment. The transitions between these states determine both the local forces experienced by each cross-bridge and the rate of ATP utilisation associated with the number of times each cross-bridge detaches from the thin filament and hydrolyses a subsequent ATP for subsequent binding and force generation. There is no thin filament regulation in the model as Ca^{2+} regulation is not considered. So, we could not couple it to an electrophysiological model as was done in the electromechanical model in sections 3.2 and 2.1. Instead, Ca^{2+} activation/regulation is considered indirectly in the model through actin permissiveness, which can be set to values between 0 (non-permissive) and 1 (fully permissive). This implies that, in this setting, troponin/tropomyosin interactions are combined into a single variable.

Subsequently, we used as input to the model, the pre-recorded experimental $[Ca^{2+}]_i$ transient profiles of control and HCM patients (Fig. 2). These were digitised and each timepoint of the pertinent profile was run until steady state, after which the steady state value was recorded. This was done throughout the time course of each $[Ca^{2+}]_i$ transient profile. In each case, the minimum value of the $[Ca^{2+}]_i$ transient in the control condition was mapped to an actin permissiveness of 0.2 and the maximum $[Ca^{2+}]_i$ transient value was mapped to an actin permissiveness of 0.1. $[Ca^{2+}]_i$ transient values were mapped proportionally between these actin permissiveness values.

Figure 5A shows the active force in control and HCM for the $[Ca^{2+}]_i$ transient profile (inset). The force in both conditions follow closely the input $[Ca^{2+}]_i$ transient profile. This should not be the case, i.e., the force should not depend exactly on the $[Ca^{2+}]_i$ transient profile as experimental transients contain artifacts from a nonlinear response of the Ca^{2+}-sensing dyes. The $[Ca^{2+}]_i$ transient and the force should be dynamically generated from a dynamic, free running cell (model) based on the interplay of ion channels and other cellular components. Unfortunately, as discussed above, the half sarcomere model does not consider Ca^{2+} regulation

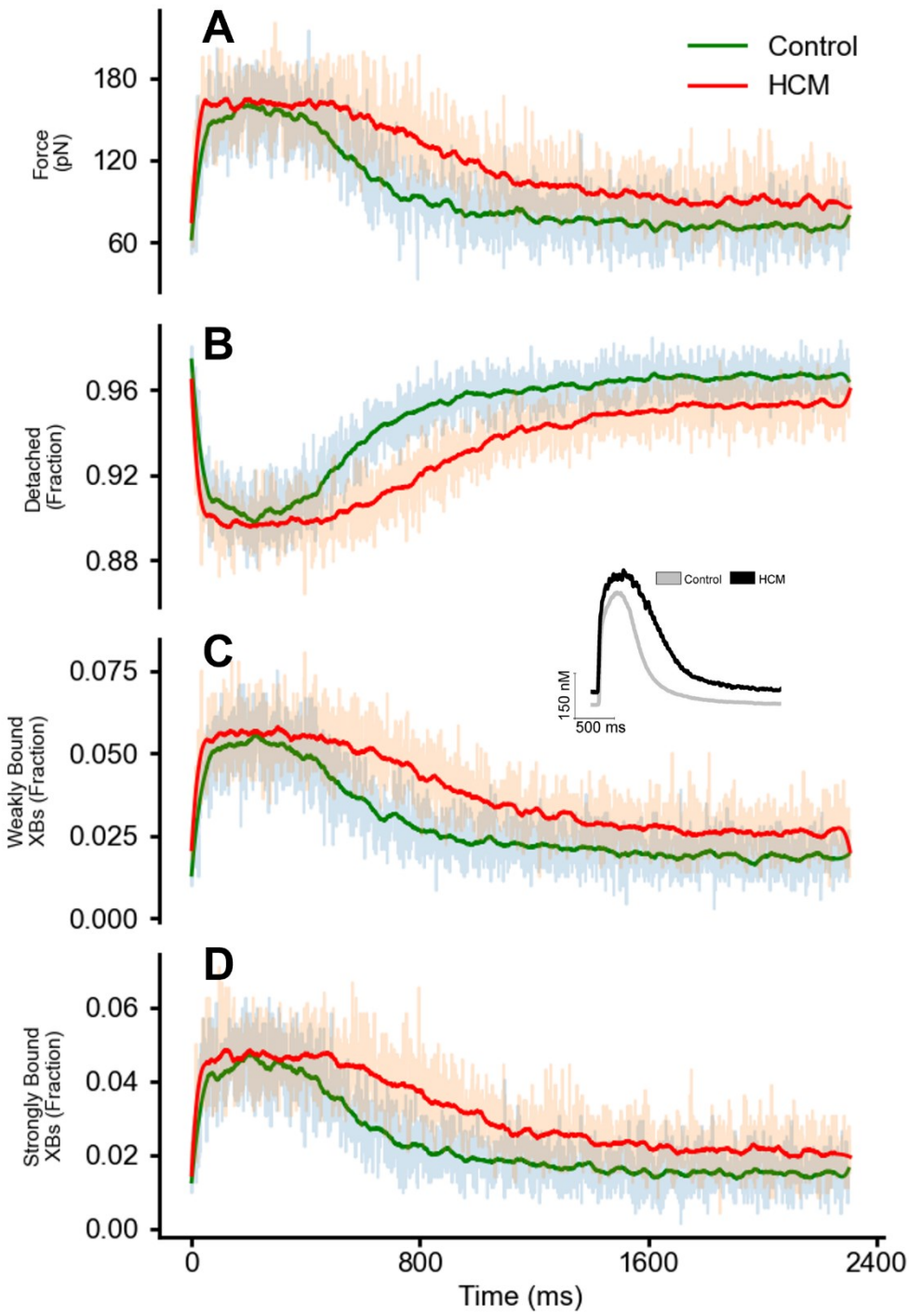

Figure 5 (Colour): Crossbridge states in control and HCM with the spatial multifilament, half sarcomere model. **(A)** The developed force in control (green) and HCM (red). **(B)** The fraction of crossbridges in the detached state during the time course of the $[Ca^{2+}]_i$ transient profile. **(C)** The fraction of crossbridges in the weakly bound state during the time course of the $[Ca^{2+}]_i$ transient profile. **(D)** The fraction of crossbridges in the strongly bound state during the time course of the $[Ca^{2+}]_i$ transient profile.

directly but only through actin permissiveness. Thus, we were unable to couple the half sarcomere model to an electrophysiology model. Nevertheless, the results are qualitatively sound.

Figures 5B, 5C and 5D show that on average, in the rest state, the control condition has ~97.5% of crossbridges in the detached state (HCM ~96%), ~1.5% in the weakly bound state (HCM ~2.4%) and ~1.5% in the strongly bound state (HCM ~1.6%). In the weakly bound state, the myosin head has broken ATP into ADP (adenosine diphosphate) and phosphate (Pi), the head has just attached to actin, but has not yet released ADP or Pi. In this state, the myosin is only partially bound to actin and little or no force is produced. The myosin head then rotates into a strongly bound configuration, which allows ADP and Pi to be released. In this state, myosin performs the primary force-producing "power stroke" of the cross-bridge cycle as it pulls on the actin filament (Lymn and Taylor, 1971). This implies that even at rest, HCM cardiomyocytes are more primed to generate force.

Throughout the time course of the active force profiles (Fig 5A), the HCM condition has more crossbridges in the detached, weakly bound and strongly bound states. At about 1000ms, when the control condition is almost completely relaxed, control has ~96% detached crossbridges (HCM ~94%) (Fig. 5B), control has ~2.5% crossbridges in the weakly bound state (HCM ~3.75%) (Fig. 5C) and in the strongly bound state, control has ~2% crossbridges while HCM has ~3%. This proportion is maintained throughout the rest of the time course of the profiles. This shows that from heartbeat to heartbeat, in the HCM condition, there are more crossbridges in the weakly bound (very low force generating) state and in the strongly bound (force generating) states compared to the control condition.

Figure S1 in the supplementary material shows the result from a second $[Ca^{2+}]_i$ transient profile from HCM patients with a MYBPC3 mutation (Fig. 2B). It shows a similar trend to the results in Fig. 5 and corroborates that HCM indeed has a higher proportion of crossbridges in the force generating states compared to control conditions.

4. Conclusion

HCM cardiomyocytes exhibited greater contractility (Figure 4) due to the combination of a) slowed $[Ca^{2+}]_i$ decay kinetics; b) reduced SERCA activity and PLB; c) greater myofilament Ca^{2+} sensitivity and (d) a higher proportion of crossbridges in force-generating states compared to the control condition. All of these combined to produce Ca^{2+} accumulation in the cytoplasm. This greater cardiomyocyte contractility is what enables the heart and in particular the left ventricle to maintain a relatively normal ejection fraction despite the wall hypertrophy and reduced chamber size seen in HCM. To achieve normal or close to normal function, the cardiomyocytes have a greater maximal oxygen consumption rate. Our results show that a relatively normal function is maintained in HCM due to Ca^{2+} handling abnormalities but at the cost of greater energy expenditure. Our results support the notion for inefficient energy utilisation as a unifying mechanism in HCM.

Declaration of Competing Interest

The authors declare that they have no known competing financial interests or personal relationships that could have appeared to influence the work reported in this paper.

References

Ashrafian, H., Redwood, C., Blair, E., Watkins, H., 2003. Hypertrophic cardiomyopathy:a paradigm for myocardial energy depletion. Trends Genet. 19, 263–268. https://doi.org/10.1016/S0168-9525(03)00081-7

Chung, J.-H., Biesiadecki, B.J., Ziolo, M.T., Davis, J.P., Janssen, P.M.L., 2016. Myofilament Calcium Sensitivity: Role in Regulation of In vivo Cardiac Contraction and Relaxation. Front. Physiol. 7, 562. https://doi.org/10.3389/fphys.2016.00562

Coppini, R., Ferrantini, C., Mugelli, A., Poggesi, C., Cerbai, E., 2018. Altered Ca2+ and Na+ Homeostasis in Human Hypertrophic Cardiomyopathy: Implications for Arrhythmogenesis. Front. Physiol. 9. https://doi.org/10.3389/fphys.2018.01391

Coppini, R., Ferrantini, C., Yao, L., Fan, P., Del Lungo, M., Stillitano, F., Sartiani, L., Tosi, B., Suffredini, S., Tesi, C., Yacoub, M., Olivotto, I., Belardinelli, L., Poggesi, C., Cerbai, E., Mugelli, A., 2013. Late Sodium Current Inhibition Reverses Electromechanical Dysfunction in Human Hypertrophic Cardiomyopathy. Circulation 127, 575–584. https://doi.org/10.1161/CIRCULATIONAHA.112.134932

Cortassa, S., Aon, M.A., Marbán, E., Winslow, R.L., O'Rourke, B., 2003. An integrated model of cardiac mitochondrial energy metabolism and calcium dynamics. Biophys. J. 84, 2734–2755. https://doi.org/10.1016/s0006-3495(03)75079-6

Del Franco, A., Ambrosio, G., Baroncelli, L., Pizzorusso, T., Barison, A., Olivotto, I., Recchia, F.A., Lombardi, C.M., Metra, M., Ferrari Chen, Y.F., Passino, C., Emdin, M., Vergaro, G., 2022. Creatine deficiency and heart failure. Heart Fail. Rev. 27, 1605–1616. https://doi.org/10.1007/s10741-021-10173-y

Haland, T.F., Hasselberg, N.E., Almaas, V.M., Dejgaard, L.A., Saberniak, J., Leren, I.S., Berge, K.E., Haugaa, K.H., Edvardsen, T., 2017. The systolic paradox in hypertrophic cardiomyopathy. Open Heart 4, e000571. https://doi.org/10.1136/openhrt-2016-000571

Helms, A.S., Tang, V.T., O'Leary, T.S., Friedline, S., Wauchope, M., Arora, A., Wasserman, A.H., Smith, E.D., Lee, L.M., Wen, X.W., Shavit, J.A., Liu, A.P., Previs, M.J., Day, S.M., 2020. Effects of *MYBPC3* loss-of-function mutations preceding hypertrophic cardiomyopathy. JCI Insight 5. https://doi.org/10.1172/jci.insight.133782

Henry, J.A., Levelt, E., Rayner, J., Hundertmark, M., Peterzan, M., Green, P., Watson, W., Lewis, A., Burrage, M., Arvidsson, P., Chamley, R., Nicol, E., Holdsworth, D., Neubauer, S., Valkovic, L., Rider, O., 2022. 143 Measuring pcr/atp as a marker of myocardial energetics across the spectrum of metabolic cardiac disease. Heart 108, A109–A110. https://doi.org/10.1136/heartjnl-2022-BCS.143

Li, S., Pan, H., Tan, C., Sun, Y., Song, Y., Zhang, X., Yang, W., Wang, X., Li, D., Dai, Y., Ma, Q., Xu, C., Zhu, X., Kang, L., Fu, Y., Xu, X., Shu, J., Zhou, N., Han, F., Qin, D., Huang, W., Liu, Z., Yan, Q., 2018. Mitochondrial Dysfunctions Contribute to Hypertrophic Cardiomyopathy in Patient iPSC-Derived Cardiomyocytes with MT-RNR2 Mutation. Stem Cell Rep. 10, 808–821. https://doi.org/10.1016/j.stemcr.2018.01.013

Lucas, D.T., Aryal, P., Szweda, L.I., Koch, W.J., Leinwand, L.A., 2003. Alterations in mitochondrial function in a mouse model of hypertrophic cardiomyopathy. Am. J. Physiol.-Heart Circ. Physiol. 284, H575–H583. https://doi.org/10.1152/ajpheart.00619.2002

Lymn, R.W., Taylor, E.W., 1971. Mechanism of adenosine triphosphate hydrolysis by actomyosin. Biochemistry 10, 4617–4624. https://doi.org/10.1021/bi00801a004

Marian, A.J., Braunwald, E., 2017. Hypertrophic Cardiomyopathy: Genetics, Pathogenesis, Clinical Manifestations, Diagnosis, and Therapy. Circ. Res. 121, 749–770. https://doi.org/10.1161/CIRCRESAHA.117.311059

O'Hara, T., Virág, L., Varró, A., Rudy, Y., 2011. Simulation of the Undiseased Human Cardiac Ventricular Action Potential: Model Formulation and Experimental Validation. PLOS Comput. Biol. 7, e1002061. https://doi.org/10.1371/journal.pcbi.1002061

Ormerod, J.O.M., Frenneaux, M.P., Sherrid, M.V., 2016. Myocardial energy depletion and dynamic systolic dysfunction in hypertrophic cardiomyopathy. Nat. Rev. Cardiol. 13, 677–687. https://doi.org/10.1038/nrcardio.2016.98

Pasipoularides, A., 2018. Challenges and Controversies in Hypertrophic Cardiomyopathy: Clinical, Genomic and Basic Science Perspectives. Rev. Espanola Cardiol. Engl. Ed 71, 132–138. https://doi.org/10.1016/j.rec.2017.07.003

Pioner, J.M., Vitale, G., Steczina, S., Langione, M., Margara, F., Santini, L., Giardini, F., Lazzeri, E., Piroddi, N., Scellini, B., Palandri, C., Schuldt, M., Spinelli, V., Girolami, F., Mazzarotto, F., van der Velden, J., Cerbai, E., Tesi, C., Olivotto, I., Bueno-Orovio, A., Sacconi, L., Coppini, R., Ferrantini, C., Regnier, M., Poggesi, C., 2023. Slower Calcium Handling Balances Faster Cross-Bridge Cycling in Human MYBPC3 HCM. Circ. Res. 132, 628–644. https://doi.org/10.1161/CIRCRESAHA.122.321956

Powers, J.D., Williams, C.D., Regnier, M., Daniel, T.L., 2018. A Spatially Explicit Model Shows How Titin Stiffness Modulates Muscle Mechanics and Energetics. Integr. Comp. Biol. 58, 186–193. https://doi.org/10.1093/icb/icy055

Ranjbarvaziri, S., Kooiker, K.B., Ellenberger, M., Fajardo, G., Zhao, M., Vander Roest, A.S., Woldeyes, R.A., Koyano, T.T., Fong, R., Ma, N., Tian, L., Traber, G.M., Chan, F., Perrino, J., Reddy, S., Chiu, W., Wu, J.C., Woo, J.Y., Ruppel, K.M., Spudich, J.A., Snyder, M.P., Contrepois, K., Bernstein, D., 2021. Altered Cardiac Energetics and Mitochondrial Dysfunction in Hypertrophic Cardiomyopathy. Circulation 144, 1714–1731. https://doi.org/10.1161/CIRCULATIONAHA.121.053575

Rice, J.J., Wang, F., Bers, D.M., de Tombe, P.P., 2008. Approximate Model of Cooperative Activation and Crossbridge Cycling in Cardiac Muscle Using Ordinary Differential Equations. Biophys. J. 95, 2368–2390. https://doi.org/10.1529/biophysj.107.119487

Rowin, E.J., Fifer, M.A., 2021. Evaluating Histopathology to Improve Our Understanding of Hypertrophic Cardiomyopathy∗. J. Am. Coll. Cardiol. 77, 2171–2173. https://doi.org/10.1016/j.jacc.2021.03.292

S, N., M, H., M, C., K, H., Jb, N., W, P., T, P., G, E., D, H., Js, I., K, K., 1997. Myocardial phosphocreatine-to-ATP ratio is a predictor of mortality in patients with dilated cardiomyopathy. Circulation 96, 2190–2196.

Santo-Domingo, J., Demaurex, N., 2010. Calcium uptake mechanisms of mitochondria. Biochim. Biophys. Acta BBA - Bioenerg., 16th European Bioenergetics Conference 2010 1797, 907–912. https://doi.org/10.1016/j.bbabio.2010.01.005

Semsarian, C., 2018. Update on the Diagnosis and Management of Hypertrophic Cardiomyopathy. Heart Lung Circ. 27, 276–279. https://doi.org/10.1016/j.hlc.2017.10.007

Spudich, J.A., 2014. Hypertrophic and Dilated Cardiomyopathy: Four Decades of Basic Research on Muscle Lead to Potential Therapeutic Approaches to These Devastating Genetic Diseases. Biophys. J. 106, 1236–1249. https://doi.org/10.1016/j.bpj.2014.02.011

Sun, Y.-B., Irving, M., 2010. The molecular basis of the steep force–calcium relation in heart muscle. J. Mol. Cell. Cardiol. 48, 859–865. https://doi.org/10.1016/j.yjmcc.2009.11.019

Tardiff, J.C., Hewett, T.E., Palmer, B.M., Olsson, C., Factor, S.M., Moore, R.L., Robbins, J., Leinwand, L.A., 1999. Cardiac troponin T mutations result in allele-specific phenotypes in a mouse model for hypertrophic cardiomyopathy. J. Clin. Invest. 104, 469–481. https://doi.org/10.1172/JCI6067

Tejado, B.S.M., Jou, C., n.d. Histopathology in HCM. Glob. Cardiol. Sci. Pract. 2018, 20. https://doi.org/10.21542/gcsp.2018.20

Tran, K., Smith, N.P., Loiselle, D.S., Crampin, E.J., 2010. A Metabolite-Sensitive, Thermodynamically Constrained Model of Cardiac Cross-Bridge Cycling: Implications for Force Development during Ischemia. Biophys. J. 98, 267–276. https://doi.org/10.1016/j.bpj.2009.10.011

Unno, K., Isobe, S., Izawa, H., Cheng, X.W., Kobayashi, M., Hirashiki, A., Yamada, T., Harada, K., Ohshima, S., Noda, A., Nagata, K., Kato, K., Yokota, M., Murohara, T., 2009. Relation of functional and morphological changes in mitochondria to myocardial contractile and relaxation reserves in asymptomatic to mildly symptomatic patients with hypertrophic cardiomyopathy. Eur. Heart J. 30, 1853–1862. https://doi.org/10.1093/eurheartj/ehp184

Wijnker, P.J.M., Sequeira, V., Kuster, D.W.D., van der Velden, J., 2019. Hypertrophic Cardiomyopathy: A Vicious Cycle Triggered by Sarcomere Mutations and Secondary Disease Hits. Antioxid. Redox Signal. 31, 318–358. https://doi.org/10.1089/ars.2017.7236

Williams, C.D., Regnier, M., Daniel, T.L., 2012. Elastic Energy Storage and Radial Forces in the Myofilament Lattice Depend on Sarcomere Length. PLOS Comput. Biol. 8, e1002770. https://doi.org/10.1371/journal.pcbi.1002770

Williams, C.D., Regnier, M., Daniel, T.L., 2010. Axial and Radial Forces of Cross-Bridges Depend on Lattice Spacing. PLOS Comput. Biol. 6, e1001018. https://doi.org/10.1371/journal.pcbi.1001018

Williams, C.D., Salcedo, M.K., Irving, T.C., Regnier, M., Daniel, T.L., 2013. The length–tension curve in muscle depends on lattice spacing. Proc. R. Soc. B Biol. Sci. 280, 20130697. https://doi.org/10.1098/rspb.2013.0697

Zorova, L.D., Popkov, V.A., Plotnikov, E.Y., Silachev, D.N., Pevzner, I.B., Jankauskas, S.S., Babenko, V.A., Zorov, S.D., Balakireva, A.V., Juhaszova, M., Sollott, S.J., Zorov, D.B., 2018. Mitochondrial membrane potential. Anal. Biochem. 552, 50–59. https://doi.org/10.1016/j.ab.2017.07.009

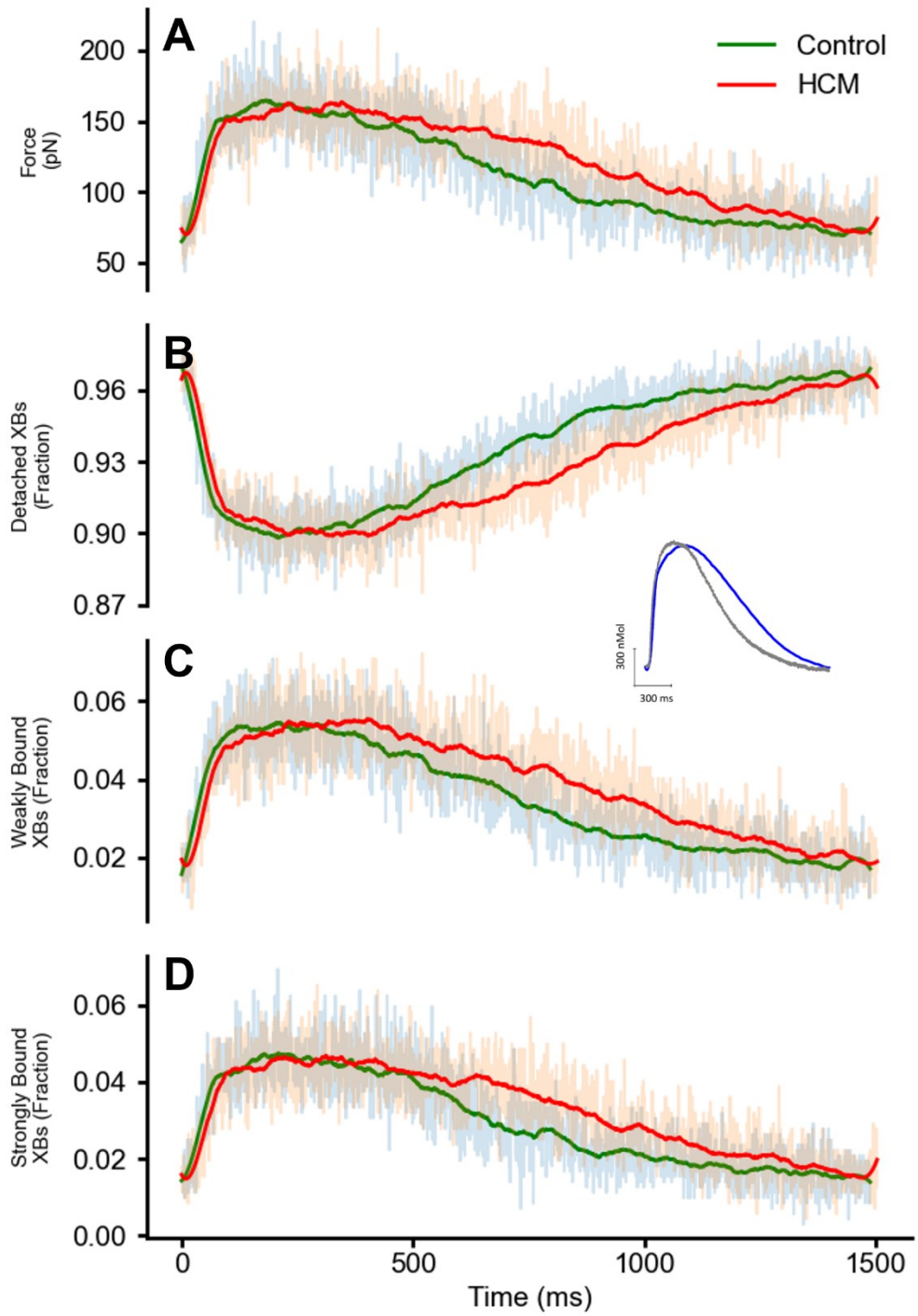

Figure S1 (Colour): Crossbridge states in control and HCM (MYBPC3 mutations) with the spatial multifilament, half sarcomere model. **(A)** The developed force in control (green) and HCM (red). **(B)** The fraction of crossbridges in the detached state during the time course of the $[Ca^{2+}]_i$ transient profile. **(C)** The fraction of crossbridges in the weakly bound state during the time course of the $[Ca^{2+}]_i$ transient profile. **(D)** The fraction of crossbridges in the strongly bound state during the time course of the $[Ca^{2+}]_i$ transient profile.